A STOCHASTIC MINIMUM-NORM APPROACH TO IMAGE AND TEXTURE INTERPOLATION

Hagai Kirshner[1], *Moshe Porat*[2], *Michael Unser*[1]

[1] Biomedical Imaging Group
École Polytechnique Fédérale de Lausanne (EPFL)
CH-1015 Lausanne, Switzerland

[2] Department of Electrical Engineering
Technion–Israel Institute of Technology
Haifa 32000, Israel

ABSTRACT

We introduce an exponential-based consistent approach to image scaling. Our model stems from Sobolev reproducing kernels, motivated by their role in continuous-domain stochastic autoregressive processes. The proposed approach imposes consistency and applies the minimum-norm criterion for determining the scaled image. We show by experimental results that the proposed approach provides images that are visually better than other consistent solutions. We also observe that the proposed exponential kernels yield better interpolation results than polynomial B-spline models. Our conclusion is that the proposed Sobolev-based image modeling could be instrumental and a preferred alternative in major image processing tasks.

1. INTRODUCTION

Image modeling is fundamental to many image processing tasks such as enhancement, restoration, analysis and compression. In the case of image interpolation, the underlying idea of current image modeling approaches corresponds to regularity constraints that are imposed on the continuous-domain image. Both theoretical and experimental studies have shown that polynomial B-spline kernels provide the best continuous-domain model for linearly interpolating a signal in terms of the SNR measure [1, 2]. Non-linear interpolation methods, on the other hand, are based on local features of edges; on wavelet and multiscale image representation; on PDE (Partial Differential Equation) models; and on the statistical properties of an image.

In this work, an alternative image modeling approach is introduced. We consider a deterministic model that imposes a less restrictive regularization constraint while utilizing the statistical properties of the image. It is suggested here to use the Sobolev space framework for this purpose. Sobolev spaces consist of smooth functions and they serve as the underlying continuous-domain model in several image processing tasks [3, 4, 5]. Further motivation for the proposed Sobolev model stems from its relation to autoregressive image modeling. The reproducing kernel Hilbert space (RKHS) property of Sobolev spaces will be shown to give rise to exponential-based interpolation kernels that correspond to generalized exponential splines introduced in [6].

Motivated by currently available acquisition devices, an image scaling operation is assumed to be consistent with the pixels of the given image. The proposed approach can assume either ideal or non-ideal sampling procedures, and in either case the sampling model remains the same for the scaled image. The pixels of the given image are interpreted by means of a continuous-domain signal in a certain sampling space, while the scaled image belongs to yet another subspace. The scaled image is not unique as there are many possible signals that comply with the consistency constraint. We identify the set of all possible consistent images and further suggest to reconstruct the signal that has the minimum possible norm. Experimental results indicate that the proposed exponential-based model provides a better alternative to currently available models, and that the proposed minimum-norm criterion outperforms visually other consistent solutions.

2. WEIGHTED SOBOLEV SPACES FOR IMAGE RECONSTRUCTION

Let $H_{\vec{\lambda}}$ be a weighted Sobolev space with weights $\vec{\lambda} = \{\lambda_n\}_1^p$. This space consists of all one-dimensional finite-energy functions defined on the real line for which their first p derivatives are of finite energy as well. The corresponding inner product is given by

$$\langle \mathbf{x}, \mathbf{y} \rangle_{H_{\vec{\lambda}}} = \sum_{n=0}^{p} \lambda_n \cdot \left\langle \mathbf{x}^{(n)}, \mathbf{y}^{(n)} \right\rangle_{L_2}, \qquad (1)$$

where the set of weights $\vec{\lambda}$ provides a positive measure for $\langle \mathbf{x}, \mathbf{x} \rangle_{H_{\vec{\lambda}}}$. The reproducing kernel of $H_{\vec{\lambda}}$ satisfies

$$\mathbf{x}(\tau) = \left\langle \mathbf{x}(t), \varphi(t - \tau; \vec{\lambda}) \right\rangle_{H_{\vec{\lambda}}} \qquad (2)$$

for every $\mathbf{x} \in H_{\vec{\lambda}}$, and it is given by the following Laplace transform

$$\Phi(s; \vec{\lambda}) = \frac{1}{\lambda_0 - \lambda_1 s^2 + \cdots + (-1)^p \cdot \lambda_p s^{2p}}. \qquad (3)$$

The poles of $\Phi(s; \vec{\lambda})$ are symmetric with respect to the imaginary axis, and if they are all simple, the corresponding inverse Laplace transform is a weighted sum

This work was supported in part by a grant from the GIF, the German-Israeli Foundation for Scientific Research and Development, by the Eshkol Fund of the Israeli Ministry of Science, and by the Ollendorff Minerva Centre. Minerva is funded through the BMBF. This work was also supported in part by the Swiss National Science Foundation under Grant 200020-121763.

 ISSN 2076-1465

of the exponential function $\alpha \cdot e^{\beta|t|}$. Such symmetric functions can be described by generalized exponential splines [6].

2.1 Ideal Sampling

The RKHS framework of Sobolev spaces suggests an orthogonal projection interpretation for ideally sampling a signal. Let $\mathbf{x}$ be an arbitrary Sobolev function and let $\{n\Delta\}$ be a set of sampling points. Then, one can identify a sampling space by shifting the reproducing kernel accordingly,

$$\mathcal{S}_{\Delta,\vec{\lambda}} = \overline{Span}\left\{\varphi(t-n\Delta;\vec{\lambda})\right\} = \overline{Span}\left\{\psi_n(t;\Delta,\vec{\lambda})\right\}, \tag{4}$$

where $\left\{\psi_n(t;\Delta,\vec{\lambda})\right\}$ is the corresponding biorthonormal set. Given the sampled version of $\mathbf{x}$, the orthogonal projection of $\mathbf{x}$ onto this subspace is

$$P_{\mathcal{S}_{\Delta,\vec{\lambda}}}\mathbf{x} = \sum_n \mathbf{x}(t_n)\cdot\psi_n(t;\Delta,\vec{\lambda}). \tag{5}$$

The RKHS property ensures that the sampled versions of both $P_{\mathcal{S}_{\Delta,\vec{\lambda}}}\mathbf{x}$ and $\mathbf{x}$ are identical as each $\psi_n(t;\Delta,\vec{\lambda})$ is interpolative. Additionally, $P_{\mathcal{S}_{\Delta,\vec{\lambda}}}\mathbf{x}$ is a minimax solution in the following sense,

$$P_{\mathcal{S}_{\Delta,\vec{\lambda}}}\mathbf{x} = \arg\min_{\hat{\mathbf{x}}} \max_{\|\mathbf{x}\|\le L,\,\{\mathbf{x}(t_n)\}} \left\|\mathbf{x}-\hat{\mathbf{x}}\right\|_{H_{\vec{\lambda}}}. \tag{6}$$

Pointwise evaluation of $P_{\mathcal{S}_{\Delta,\vec{\lambda}}}\mathbf{x}$ can be performed by vector multiplication calculation,

$$P_{\mathcal{S}_{\Delta,\vec{\lambda}}}\mathbf{x}(\tau) = p^T\cdot G^{-1}\cdot b, \tag{7}$$

where $p[n]=\mathbf{x}(n\Delta)$, $b[n]=\varphi(n\Delta-\tau,\vec{\lambda})$ and $G(m,n)=\varphi((m-n)\Delta,\vec{\lambda})$ is a Gram matrix.

2.2 Non-Ideal Sampling

Non-ideal samples of a continuous-domain signal are given here by,

$$p[n] = \langle \mathbf{x}(t), \mathbf{s}(t-n\Delta)\rangle_{L_2}, \tag{8}$$

where $\mathbf{s}(t)$ is a sampling function that characterizes the acquisition device. In cases where $\mathbf{x}$ is a Sobolev signal, the L_2 inner product can be alternatively described by a Sobolev inner product

$$p[n] = \left\langle \mathbf{x}(t), \tilde{\varphi}(t-n\Delta,\vec{\lambda})\right\rangle_{H_{\vec{\lambda}}}, \tag{9}$$

where

$$\tilde{\varphi}(t,\vec{\lambda}) = \left\{\varphi(\tau;\vec{\lambda}) * \mathbf{s}(\tau)\right\}(t) \tag{10}$$

and $*$ denotes convolution. It then follows that a non-ideal sampling model defines a modified sampling space,

$$\widetilde{\mathcal{S}}_{\Delta,\vec{\lambda}} = \overline{Span}\left\{\tilde{\varphi}(t-n\Delta;\vec{\lambda})\right\} = \overline{Span}\left\{\tilde{\psi}_n(t;\Delta,\vec{\lambda})\right\}. \tag{11}$$

In this case, however, the biorthogonal functions are not interpolative. Instead, they comply with a generalized interpolation criterion given by

$$\left\langle \tilde{\psi}_n(t;\Delta,\vec{\lambda}), \mathbf{s}_m\right\rangle_{L_2} = \delta[n-m]. \tag{12}$$

The minimum norm property and the minimax optimality of $P_{\widetilde{\mathcal{S}}_{\Delta,\vec{\lambda}}}\mathbf{x}$ are still valid, though.

3. MMSE SIGNAL INTERPOLATION

The Laplace transform of (3) may also originate from an autocorrelation function of a continuous-domain autoregressive stochastic process. As a matter of fact, both the reproducing kernel $\varphi(t,\vec{\lambda})$ and the autocorrelation function $r(t;\vec{\lambda})$ have a similar role in signal interpolation. The minimum mean square error (MMSE) linear estimator of $\mathbf{x}(\tau)$ is given by,

$$\hat{\mathbf{x}}(\tau) = \sum_n a[n]\cdot\mathbf{x}(t_n), \tag{13}$$

where a is a set of coefficients that is determined by the orthogonality principle of linear estimators. It follows that

$$\sum_m a[m]\cdot r(t_m-t_n;\vec{\lambda}) = r(\tau-t_n;\vec{\lambda}) \tag{14}$$

holds for every coordinate t_n, where $r(t;\vec{\lambda})$ is the autocorrelation function of $\mathbf{x}$. Denoting $G(m,n)=r(t_m-t_n;\vec{\lambda})$, $b[n]=r(\tau-t_n;\vec{\lambda})$ and $p[n]=\mathbf{x}(t_n)$, the linear estimation of $\mathbf{x}(\tau)$ is identical to $P_{\mathcal{S}_{\Delta,\vec{\lambda}}}\mathbf{x}(\tau)$.

This equivalence between the Sobolev-based deterministic model and the autoregressive stochastic model can be utilized for choosing the optimal weights $\vec{\lambda}$ of (1). Given a sampled signal, one can estimate the autoregressive parameters of the continuous-domain process; determine the autocorrelation function $r(t)$; and set $\varphi(t)=r(t)$. For a uniformly sampled signal, it is suggested here to assume a discrete-domain autoregressive process and extract its parameters by the least square estimation method. In such a case, the z-transform of the autocorrelation sequence would consist of poles that appear in reciprocal pairs $\{z_n, 1/z_n\}_{n=1}^{p}$ where $|z_n|<1$. The poles of the continuous-domain process will be assumed then to be $\{s_n = ln(z_n)\}_{n=1}^{2p}$, for which $\{\lambda_n\}_{n=0}^{p}$ can be readily determined. Two-dimensional signals will be assumed to have a separable autocorrelation function and the horizontal autocorrelation function will be estimated separately from the vertical one.

The proposed approach posses the simplicity of linear methods while further pushing the paradigm of super resolution methods by adapting itself to the given signal [7]. On top of that, it provides a continuous-domain signal that takes the sampling process into account.

4. CONSISTENT IMAGE SCALING

Motivated by typical acquisition devices, image scaling is considered to be a zoom-in/zoom-out operation, for which the same acquisition device is used for every scale.

It follows that scaling an image corresponds to reacquiring the original signal by scaled versions of the sampling functions that characterize the device. These sampling functions are not necessarily Dirac distributions, i.e., ideal sampling, but finite-support functions that describe the non-ideal nature of the device, as is the case of zero-order-hold (ZOH) sampling for example.

A consistent approach is suggested here for image scaling. This approach can take either ideal or non-ideal sampling procedures. In an ideal sampling case, the pixels of the scaled image correspond to point-wise evaluation of the reconstructed signal, whereas for non-ideal sampling procedures, the pixels correspond to averaging the reconstructed signal over scaled intervals. The sampling step of the given image is assumed to be of unit size and the sampling step of the scaled image is assumed to be Δ. The consistent approach would reconstruct a signal for which its unit-step sampled version would be consistent with the pixels of the given image (Figure 1). Furthermore, this signal should be as close as possible to $P_{\widetilde{\mathcal{S}}_{\Delta,\vec{\lambda}}}\mathbf{x}$, which is the image one would get from $\mathbf{x}$ itself,

$$\min_{\hat{\mathbf{x}}} \max_{\substack{\|\mathbf{x}\|_{H_{\vec{\lambda}}}\leq L,\\ P_{\widetilde{\mathcal{S}}_{1,\vec{\lambda}}}\hat{\mathbf{x}}=P_{\widetilde{\mathcal{S}}_{1,\vec{\lambda}}}\mathbf{x}}} \left\| P_{\widetilde{\mathcal{S}}_{\Delta,\vec{\lambda}}}\mathbf{x}-\hat{\mathbf{x}}\right\|_{H_{\vec{\lambda}}}. \tag{15}$$

It holds that $P_{\widetilde{\mathcal{S}}_{1,\vec{\lambda}}}\hat{\mathbf{x}}$ is a shifted balanced set,

$$P_{\widetilde{\mathcal{S}}_{\Delta,\vec{\lambda}}}\mathbf{x}=P_{\widetilde{\mathcal{S}}_{\Delta,\vec{\lambda}}}P_{\widetilde{\mathcal{S}}_{1,\vec{\lambda}}}\mathbf{x}+P_{\widetilde{\mathcal{S}}_{\Delta,\vec{\lambda}}}P_{\widetilde{\mathcal{S}}^{\perp}_{1,\vec{\lambda}}}\mathbf{x}, \tag{16}$$

and a minimax solution would minimize the distance to the center of this set, $P_{\widetilde{\mathcal{S}}_{\Delta,\vec{\lambda}}}P_{\widetilde{\mathcal{S}}_{1,\vec{\lambda}}}\mathbf{x}$, which is known. On the other hand, admissible consistent solutions form a shifted balanced set, too. Its center is $P_{\widetilde{\mathcal{S}}_{1,\vec{\lambda}}}\mathbf{x}$; adding a vector in $\widetilde{\mathcal{S}}^{\perp}_{1,\vec{\lambda}}$ would still result in a consistent solution. As theses two centers do not necessarily coincide, the minimax solution is dependent on the norm of the original signal L, which in practice is unknown. It is therefore suggested here to relax the minimax constraint and find a consistent solution in $\widetilde{\mathcal{S}}_{\Delta,\vec{\lambda}}$ that has the minimum possible norm. That is,

$$\min_{\hat{\mathbf{x}}\in\widetilde{\mathcal{S}}_{\Delta,\vec{\lambda}}} \left\|\hat{\mathbf{x}}\right\|_{H_{\vec{\lambda}}} \text{ s.t. } P_{\widetilde{\mathcal{S}}_{1,\vec{\lambda}}}\hat{\mathbf{x}}=P_{\widetilde{\mathcal{S}}_{1,\vec{\lambda}}}\mathbf{x}. \tag{17}$$

Consistent sampling gives rise to oblique projections [8, 9]. Such projections are uniquely defined if and only if the reconstruction and the sampling spaces comply with a direct-sum relation. However, this is not the case here. For image up-scaling ($\Delta < 1$), for example, there might be several possible signals in the reconstruction space $\widetilde{\mathcal{S}}_{\Delta,\vec{\lambda}}$ that comply with the consistency requirement. A consistent solution can be written as $\hat{\mathbf{x}}=\hat{\mathbf{x}}_1+\hat{\mathbf{x}}_2$, where

$$\hat{\mathbf{x}}_1 \in \widetilde{\mathcal{S}}_{\Delta,\vec{\lambda}} \Big\backslash \left(\widetilde{\mathcal{S}}_{\Delta,\vec{\lambda}} \bigcap \widetilde{\mathcal{S}}^{\perp}_{1,\vec{\lambda}}\right) \tag{18}$$

is consistent with the known samples and $\hat{\mathbf{x}}_2 \in \widetilde{\mathcal{S}}^{\perp}_{1,\vec{\lambda}}$.

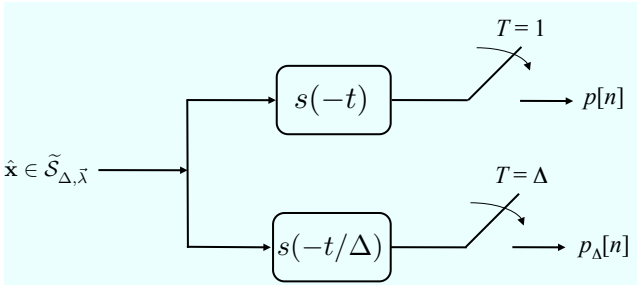

Figure 1: The proposed image scaling approach. The reconstructed signal $\hat{\mathbf{x}}$ should be consistent with the known pixels (top branch) and should have a minimum norm property. The pixels of the scaled image correspond to sampling $\hat{\mathbf{x}}$ at the new grid while using scaled sampling functions (bottom branch).

Theorem 1 *Let $\mathbf{x} \in H_{\vec{\lambda}}$ be given by its unit-interval samples and let $\widetilde{\mathcal{S}}_{1,\vec{\lambda}}$ be the corresponding sampling space. Let also $\widetilde{\mathcal{S}}_{\Delta,\vec{\lambda}}$ be a sampling space corresponding to a sampling interval Δ as given by (11). If $\Delta < 1$ (up-scaling), then a consistent reconstruction of $\mathbf{x}$ in the sense of (17) is the oblique projection of $P_{\widetilde{\mathcal{S}}_{1,\vec{\lambda}}}\mathbf{x}$ onto the space*

$$\widetilde{\mathcal{S}}_{\Delta,\vec{\lambda}} \Big\backslash \left(\widetilde{\mathcal{S}}_{\Delta,\vec{\lambda}} \bigcap \widetilde{\mathcal{S}}^{\perp}_{1,\vec{\lambda}}\right), \tag{19}$$

having a null space $\widetilde{\mathcal{S}}^{\perp}_{1,\vec{\lambda}}$.

The approach yields a signal that has the following properties: 1) It resides in a vector space that is determined by the sampling process and by the stochastic properties of the given image. 2) Its unit-interval sampled version is consistent with the given image. 3) It is minimum norm. The scaled image is obtained then by re-sampling this signal at the required grid. The proposed image scaling algorithm is described next. The orthogonal projection of $\mathbf{x}$ onto $\widetilde{\mathcal{S}}_{1,\vec{\lambda}}$ is given by

$$P_{\widetilde{\mathcal{S}}_{1,\vec{\lambda}}}\mathbf{x}=\sum_{n=0}^{N-1} a[n]\cdot\tilde{\varphi}(t-n), \tag{20}$$

where $a = G^{-1}p$. $G(m,n)=\tilde{\varphi}(m-n)$ is the Gram matrix of the sampling functions and p is a vector of the known samples/pixels. The reconstructed signal is given by

$$\hat{\mathbf{x}}=\sum_{m=0}^{M-1} b[n]\cdot\tilde{\varphi}(t-n\Delta), \tag{21}$$

and there need to be M linear equations for determining the coefficients b. N equations are given by the consistency constraint,

$$A_{N\times M}\cdot\begin{bmatrix} b[0] \\ \vdots \\ b[M-1] \end{bmatrix}=\begin{bmatrix} p[0] \\ \vdots \\ p[N-1] \end{bmatrix}, \tag{22}$$

where $A(n,m)=\tilde{\varphi}(n-m\Delta)$. The additional $M-N$ equations originate from the constraint

$$\hat{\mathbf{x}} \notin \widetilde{\mathcal{S}}_{\Delta,\vec{\lambda}} \bigcap \widetilde{\mathcal{S}}^{\perp}_{1,\vec{\lambda}}. \tag{23}$$

The basis functions of this space are determined by the null space of A, and the reconstructed signal should be orthogonal to each one of them. This is expressed by

$$B_{(M-N)\times M} \cdot \begin{bmatrix} b[0] \\ \vdots \\ b[M-1] \end{bmatrix} = \begin{bmatrix} 0 \\ \vdots \\ 0 \end{bmatrix}, \qquad (24)$$

where $B(m,n) = \sum_{k=0}^{M-1} \nu_m[k] \cdot \tilde{\varphi}(k\Delta - n\Delta)$ and where ν_m is the mth vector in the null space of A. In cases where $\widetilde{\mathcal{S}}_{1,\vec{\lambda}} \in \widetilde{\mathcal{S}}_{\Delta,\vec{\lambda}}$, the reconstructed signal is equal to $P_{\widetilde{\mathcal{S}}_{1,\vec{\lambda}}}\mathbf{x}$. For example, for an ideal sampling model and for cases where the grid of the scaled image contains the grid of the given image, the proposed approach yields the sampled version of $P_{\widetilde{\mathcal{S}}_{1,\vec{\lambda}}}\mathbf{x}$, which accounts for standard resampling. This is not the case, however, for other sampling grids (Figure 2) or for non-ideal sampling models.

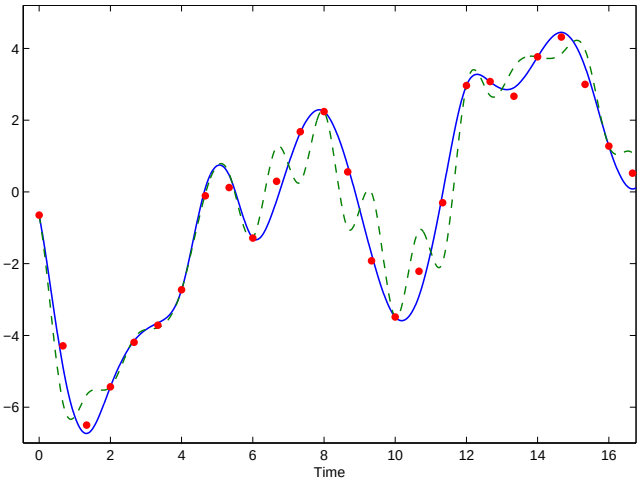

Figure 2: MMSE interpolation of an autoregressive process by a non-integer factor. A continuous-domain autoregressive process has been sampled on a unit sampling grid. The same stochastic process was then sampled at a finer grid of $\Delta = 2/3$ (dots). Shown here are an exponential-based (solid) and a polynomial-based (dashed) reconstructed signals that originate from the unit-interval sample values. Both signals are consistent with the known samples of the unit-interval grid and they are of minimum norm. The proposed exponential model provides a better approximation to the true values of the process than does the polynomial model as indicated by the MSE values of their sampled versions: 0.0982 vs. 0.5683 respectively. It is noted that every third sample in the figure coincides with both signals as it coincides with the unit-interval sampling grid. The poles of the continuous-domain process are $\vec{\lambda} = \{-0.5, -1\}$.

5. EXPERIMENTAL RESULTS

Consistent image scaling experiment were carried out using the proposed model and the polynomial B-spline model. An ideal sampling procedure was considered, i.e., $s(t) = \delta(t)$, for which down-scaling was performed by sampling the original image at a three-times coarser sampling grid. The down-scaled image was then up-scaled by a factor of $\Delta = 2/3$ using both models. Both reconstructed signals are consistent with the known pixel values and are of minimum norm. The up-scaled image was then compared with pixel values of the original image taken on a two-times coarser sampling grid. Numerical comparison is given in Table 1. As reflected from the table, the proposed model provides higher SNR values when considering various types of images and texture [10] as it adopts the Sobolev weights to the given image. SNR values were carried out while excluding boundary pixels of the image; the width of the boundary region was 10% of the image size. Shown also in Table 1 are VIF (Visual Fidelity Information Fidelity) values [11]. Figure 3 provides visual comparison between minimum-norm and non minimum-norm signals, indicating that the proposed minimum-norm criterion is preferable in this regard.

Image	**SNR [dB] (VIF)**	
	Polynomial B-spline $L = 4$**, cubic**	**Proposed Model** $p = 2$
Autoregressive	22.09 (0.62)	24.66 (0.69)
Lena	22.15 (0.47)	22.39 (0.50)
Fishing Boat	18.77 (0.45)	18.84 (0.46)
Alliums	19.54 (0.51)	19.70 (0.54)
Rose	25.49 (0.39)	25.87 (0.42)
D23	17.37 (0.39)	17.76 (0.40)
D28	15.93 (0.34)	15.96 (0.35)
D75	18.84 (0.39)	19.37 (0.41)

Table 1: A comparison of consistent image scaling. The original image was down-sampled by a factor of three using the ideal sampling model and was then up-scaled by a factor of $\Delta = 2/3$. The up-scaled image is consistent with the down-sampled image. The up-scaled image is compared here with pixel values of the original image taken on a doubly-spaced sampling grid . VIF indicates Visual Information Fidelity according to [11].

6. CONCLUSIONS

A reproducing-kernel Hilbert space approach has been proposed for image and texture scaling. Sobolev functions, which are dense in L_2, provide a useful framework for this purpose. The reproducing kernels of Sobolev spaces have been shown to be of an exponential type. These kernels are related to autoregressive processes, suggesting a method for determining the proper Sobolev weights for a given image. Image scaling operations were assumed to be consistent with the pixels of the given image; these pixels can be either ideal or non-ideal samples of the continuous-domain image. The proposed approach assumes that images of different resolutions originate from a single continuous-domain signal while being acquired by properly scaled versions of a single set of sampling functions. A minimum-norm criterion was also suggested for reconstructing the scaled image, giving rise to an oblique projection operation in Sobolev spaces. Experimental results show that the proposed approach can provide a preferred alternative approach

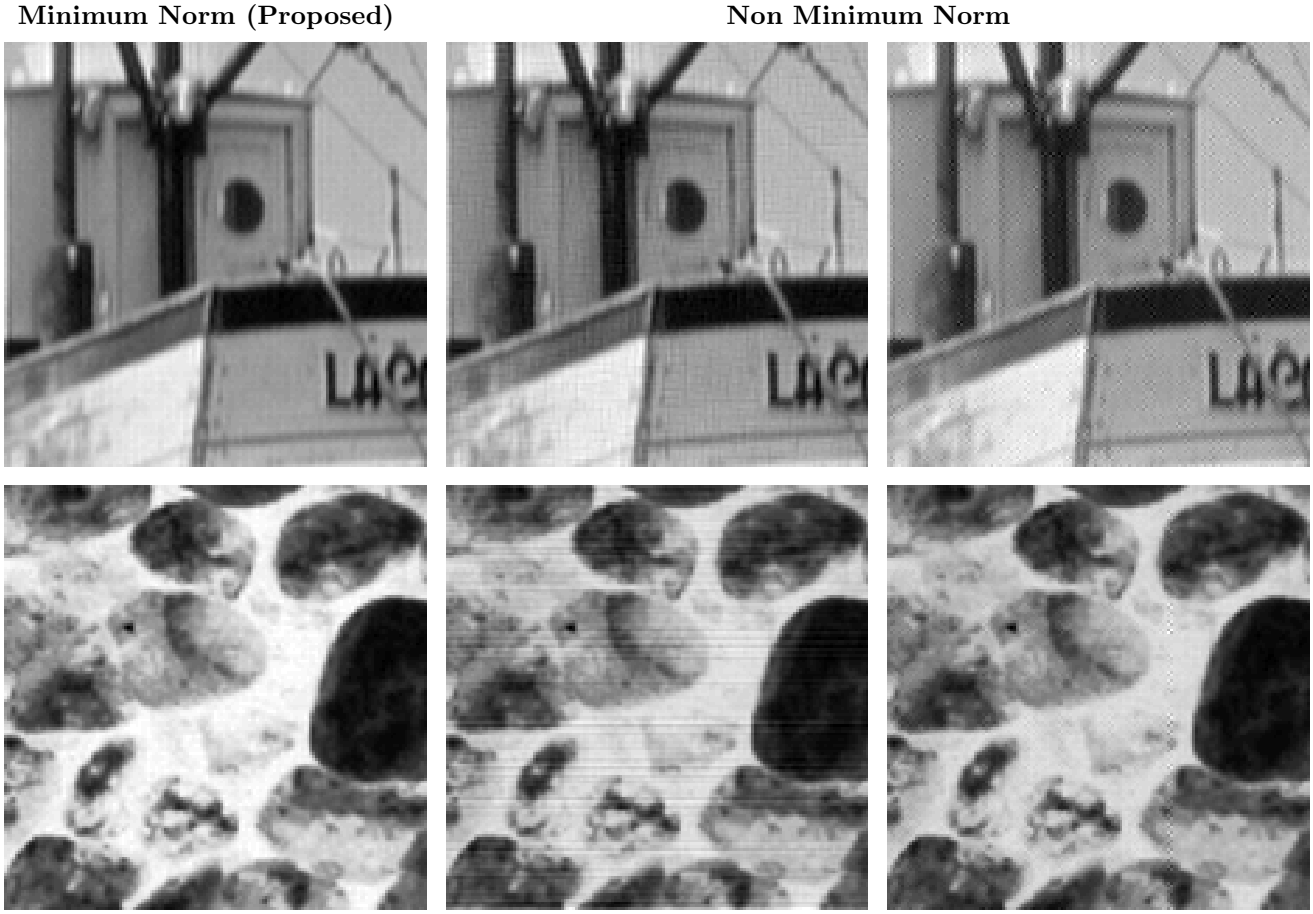

Figure 3: A visual comparison of consistent image scaling. Shown here are portions of the Fishing Boat image (first row) and of the D23 Brodatz image (second row) having been up-scaled by a factor of $\Delta = 2/3$. The left column corresponds to a consistent reconstruction having the minimum norm property. The other two columns are consistent but not of minimum norm (the ℓ_2 norm is larger by no more than 1%). Every third pixel has the same value for all of the images as they coincide with pixels of the original image. The non minimum norm images were generated by randomly adding a function from $\widetilde{\mathcal{S}}_{\Delta,\vec{\chi}} \cap \widetilde{\mathcal{S}}^{\perp}_{1,\vec{\chi}}$.

to image modeling in general, and in particular to image scaling tasks.

REFERENCES

[1] T. Blu, P. Thévenaz, and M. Unser, "MOMS: Maximal-order interpolation of minimal support," *IEEE Trans. Image Processing*, vol. 10, pp. 1069–1080, July 2001.

[2] E. H. W. Meijering, W. J. Niessen, and M. A. Viergever, "Quantitative evaluation of convolution-based methods for medical image interpolation," *Med. Image Anal.*, vol. 5, no. 2, pp. 111–126, 2001.

[3] G. Sundaramoorthi, A. Yezzi, and A. Mennucci, "Coarse-to-fine segmentation and tracking using Sobolev active contours," *IEEE Trans. Pattern Analysis and Machine Intelligence*, vol. 30, no. 5, pp. 851–864, May 2008.

[4] T. F. Chan and J. Shen, *Image Processing And Analysis: Variational, PDE, Wavelet, And Stochastic Methods*. SIAM, 2005.

[5] H. Kirshner and M. Porat, "On the approximation of L_2 inner products from sampled data," *IEEE Trans. Signal Processing*, vol. 55, no. 5, pp. 2136–2144, May 2007.

[6] M. Unser, "Cardinal exponential splines: part II - think analog, act digital," *IEEE Trans. Signal Processing*, vol. 53, no. 4, pp. 1439 – 1449, Apr. 2005.

[7] J. D. van Ouwerkerk, "Image super-resolution survey," *Image and vision Computing*, vol. 24, no. 10, pp. 1039–1052, October 2006.

[8] M. Unser and A. Aldroubi, "A general sampling theory for nonideal acquisition devices," *IEEE Trans. Signal Processing*, vol. 42, no. 11, pp. 2915–2925, Nov. 1994.

[9] T. Dvorkind and Y. C. Eldar, "Robust and consistent sampling," *IEEE Signal Processing Letters*, vol. 16, no. 9, pp. 739–742, September 2009.

[10] M. Porat and Y. Y. Zeevi, "Localized texture processing in vision: analysis and synthesis in the Gaborian space," *IEEE Trans. Biomedical Engineering (BME)*, vol. 36, no. 11, pp. 115–129, 1989.

[11] H. R. Sheikh and A. C. Bovik, "Image information and visual quality," *IEEE Trans. Image Processing*, vol. 15, no. 2, pp. 430–444, February 2006.